

Multivariate Signal Denoising Based on Generic Multivariate Detrended Fluctuation Analysis

Khuram Naveed, Sidra Mukhtar and Naveed ur Rehman

Abstract—We propose a generic multivariate extension of detrended fluctuation analysis (DFA) that incorporates interchannel dependencies within input multichannel data to perform its long-range correlation analysis. We next demonstrate the utility of the proposed method within multivariate signal denoising problem. Particularly, our denoising approach first obtains data driven multiscale signal representation via multivariate variational mode decomposition (MVMD) method. Then, proposed multivariate extension of DFA (MDFA) is used to reject the predominantly noisy modes based on their randomness scores. The denoised signal is reconstructed using the remaining multichannel modes albeit after removal of the noise traces using the principal component analysis (PCA). The utility of our denoising method is demonstrated on a wide range of synthetic and real life signals.

I. INTRODUCTION

MULTI sensor data acquisition systems have become widespread in many application areas including medical diagnosis, health monitoring, geophysics, weather forecasting, fault diagnosis etc. Within those systems, a network of synchronized sensors is used to record signals originating from physical system(s) resulting in interdependent multichannel observations. Those observations, denoted by $\mathbf{x}_i \in \mathcal{R}^m$, could be mathematically modelled as being composed of the desired signal in combination with unwanted noise, as given below

$$\mathbf{x}_i = \mathbf{s}_i + \boldsymbol{\psi}_i, \quad \forall \quad i = 1, \dots, N, \quad (1)$$

where $\mathbf{s}_i \in \mathcal{R}^m$ denotes a desired multivariate signal observation at time index i , while $\boldsymbol{\psi}_i \in \mathcal{R}^m$ denotes a multivariate additive noise observation which is assumed to be independent and identically distributed by zero mean multivariate Gaussian distribution $\mathcal{N}_m(\mathbf{0}, \Sigma)$ with covariance matrix Σ .

Several methods have been proposed in literature to estimate true multivariate signal \mathbf{s}_i from raw signal recordings \mathbf{x}_i . Most of those denoising methods are direct multichannel extensions of the popular multiscale approaches that have worked extremely well on univariate (single-channel data). For instance, in [1], the sparsity of discrete wavelet transform (DWT) is exploited to reject noise via a multichannel expansion of the universal threshold [2]. Similarly, [3] utilizes a variant of the DWT namely synchrosqueezing wavelet transform for multivariate noise removal. Apart from that, multivariate empirical mode decomposition (MEMD) [4], [5] has also been used for multivariate signal denoising by employing a univariate interval thresholding function [6] and by using more accurate multivariate thresholding function based on Mahalanobis distance (MD) measure [7].

K. Naveed, S. Mukhtar and N. ur Rehman are with the Department of Electrical and Computer Engineering, COMSATS University Islamabad (CUI), Islamabad, Pakistan (emails: khuram.naveed@comsats.edu.pk, sidra-mukhtar018@gmail.com, naveed.rehman@comsats.edu.pk).

Recently, variational mode decomposition (VMD) algorithm [8] and its multivariate extension [9] have emerged as more powerful new tools as compared to (M)EMD, owing to their sound mathematical foundation. Consequently, (M)VMD have been adopted for signal denoising applications: For instance, in [10], Hausdorff distance has been used in combination with MVMD for multichannel signal denoising. A more rigorous approach, in the context of univariate data, employs detrended fluctuation analysis (DFA) [11] to identify the VMD modes with predominant noise, which are subsequently removed to obtain the denoised signal [12]. The robustness of this approach stems from the ability of DFA to accurately estimate long-range correlations in a time series which results in automatic detection of the noisy modes within VMD.

In its original form, DFA only caters for single-channel time series data. While its multichannel extension exists [13], it processes each data channel in isolation thereby ignoring inter-channel correlations within multivariate data. To that end, we develop a novel and generic multichannel extension of DFA, termed MDFA in the sequel, that fully incorporates inter-channel correlations within data by utilizing Mahalanobis distance measure. Using that extension, we propose a novel multichannel multiscale denoising method that first uses MVMD to decompose a multivariate data into multiple frequencies and then identifies (and rejects) noisy modes using MDFA.

II. MULTIVARIATE VARIATIONAL MODE DECOMPOSITION

Multivariate VMD [9] is a generic multichannel extension of the VMD algorithm that decomposes a multivariate signal $\mathbf{x}_i \in \mathcal{R}^m$ into K number of predefined multivariate modulated oscillations $\mathbf{u}_{k,i} \in \mathcal{R}^m$ which are based on a common frequency component across all channels.

$$\mathbf{x}_{i_n} = \sum_{k=1}^K \mathbf{u}_{k,i_n} \quad (2)$$

The objective function within MVMD has been defined as the bandwidth of K number of multivariate modulated oscillations across all channels. That is subject to the multiple constraints of signals across multiple channels being equal to the sum of the decomposed components. The resulting optimization problem is given below.

$$\underset{u_{k,n}, w_k}{\text{minimize}} \left\{ \sum_{k=1}^K \sum_{n=1}^m \left\| \partial_t \left[u_{k,i_n}^+ e^{-jw_k i} \right] \right\|_2^2 \right\}, \quad (3)$$

where $u_{k,i}^n$ denote multichannel band-limited intrinsic mode functions (BLIMFs) represented as a function of modulated multivariate oscillation u_{k,i_n}^+ , assuming a common frequency component $w_k = \frac{d\phi_k}{dt}$. Owing to that MVMD avoids the mode mixing problem otherwise observed in MEMD that makes MVMD useful in a variety of applications including denoising.

III. DETRENDED FLUCTUATION ANALYSIS

The detrended fluctuation analysis (DFA) is widely used to estimate the extent of long-range correlations in a non-stationary time series because it circumvents the artefacts of nonstationarity (e.g., local trend, noise etc.) which cause spurious scores in the otherwise used Hurst exponent method [11]. Specifically, DFA estimates a power law *scaling exponent* by observing natural variability of the fluctuations around the local trend with change in the time scale. In this regard, intrinsic fluctuations of a (nonstationary) time series are extracted by *detrending* the slowly oscillating background that causes spurious scores [14]. The steps involved within DFA are described below:

Given a time series $x_i \forall i = 1, \dots, N$, its normalized cumulative sum is obtained as follows: $y_i = \frac{1}{N} \sum_{i=1}^N (x_i - \bar{x})$, where \bar{x} denotes the mean. The resulting profile y_i is then divided into $N_s = N/s$ segments of equal length s from both ends in order to estimate the local trend \tilde{y}_i using the least squares polynomial fit (of a given order). Finally, a fluctuation function $F(s)$ is obtained based on the detrend $y_i - \tilde{y}_i$

$$F(s) = \sqrt{\frac{1}{2N_s} \sum_{v=1}^{2N_s} \left(\frac{1}{s} \sum_{i=1}^s (y_i - \tilde{y}_i)^2 \right)}. \quad (4)$$

Note that $F(s)$ is the root mean of local (segment) variances that is expected to increase with increase in the time scale s . This increase in $F(s)$, when described using the power law relation of the time scale s reflects on the long range correlations of the time series [15]. Specifically, the scale exponent α indicates long-range correlations if $\alpha > 0.5$ while the cases of $\alpha = 0.5$ and $\alpha < 0.5$ suggest no-correlations and short-range correlations respectively. Moreover, α informs about the degree of smoothness of a time series, i.e., a higher α indicates the presence of slow fluctuations while a lower α hints at rapid fluctuations [16]. The resulting insight gained via DFA renders it suitable in many signal processing related applications involving signal analysis [17] and denoising [12].

A multichannel DFA is presented in [13] using a straightforward multichannel generalization of (3) which is given by

$$F'_m(s) = \sqrt{\frac{1}{2N_s} \sum_{v=1}^{2N_s} \left(\frac{1}{s} \sum_{i=1}^s \sum_{n=1}^m (y_{i_n} - \tilde{y}_{i_n})^2 \right)}, \quad (5)$$

where y_{i_n} and \tilde{y}_{i_n} respectively denote the profile and polynomial fit for the n th channel. Observe from (3) that the Euclidean norm of each m -variate error observation is used to formulate a multichannel fluctuation function $F'_m(s)$ which completely disregards the cross-channel correlations and may lead to spurious scores.

IV. PROPOSED METHODOLOGY

This section outlines a multiscale multivariate signal denoising framework based on MVMD and MDFA. For this purpose, we first describe the proposed multichannel extension of DFA that underpins our denoising framework.

A. Multichannel Extension of DFA

The existing multichannel DFA [13] completely disregards the cross-channel correlations of a multivariate time series and

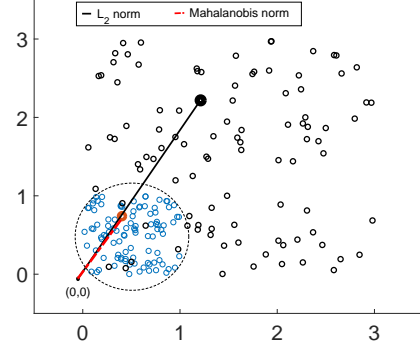


Fig. 1: Rationale behind the use of MD as a norm over the Euclidean distance (ED) based classical L_2 norm: Observe that MD (depicted using red line) computes ED after relocating the multidimensional data points (originally plotted via 'o' in black) to a unit variance circle (plotted via 'o' in blue) by incorporating the correlations between the dimensions (channels) and performing variance normalization across each dimensions. Hence, MD is sensitive to cross-correlations but it is not perturbed by the variance bias across dimensions.

may lead to spurious scores especially for cross-correlated multichannel data. To address this issue, we propose a novel multichannel extension of the (1D) DFA that considers cross-correlations via Mahalanobis distance (MD) measure and may be seen as a generalization of [13]. The steps involved in our new MDFA are discussed below:

Given a multivariate time series $\mathbf{x}_i \forall i = 1, \dots, N$ where $\mathbf{x}_i = [x_{i_1}, \dots, x_{i_m}]^T \in \mathcal{R}^m$ represents an m -variate observation at time index i , the cumulative sum \mathbf{y}_i is computed via

$$\mathbf{y}_i = \frac{1}{N} \sum_{i=1}^N (\mathbf{x}_i - \bar{\mathbf{x}}), \quad (6)$$

where $\bar{\mathbf{x}} = \frac{1}{N} \sum_{i=1}^N \mathbf{x}_i$ denotes the multichannel mean.

Next, the signal $\mathbf{y}_i = \{y_{i_n}\}_{n=1}^m$ for all $i = 1, \dots, N$, is divided in $2N_s$ spatial segments by cutting it into $N_s = N/s$ segments of equal size starting from both ends of the series. Now, the local trend $\tilde{\mathbf{y}}_i = \{\tilde{y}_{i_n}\}_{n=1}^m$ is estimated based on the quadratic polynomial fit of each channel

$$\tilde{y}_{i_n} = a_n \cdot i^2 + b_n \cdot i + c_n, \quad i = 1, \dots, s, \quad (7)$$

where a_n, b_n, c_n denote the coefficients required for the least square fit $\tilde{y}_{i_n} \sim y_{i_n}$. Here, quadratic polynomial is used to estimate the slowly varying background trend albeit a higher order polynomial fit could also be used.

Definition 1 (Mahalanobis norm): Let Σ denote a symmetric and positive definite covariance matrix of vector observations $\{\mathbf{z}_i\}_{i=1}^N$, we define the Mahalanobis norm $\|\mathbf{z}_i\|_{\Sigma} = \sqrt{\mathbf{z}_i^T \Sigma^{-1} \mathbf{z}_i}$ that satisfies the following properties of a norm on that vector space \mathcal{Z} , i.e.,

- 1) $\|\mathbf{z}\|_{\Sigma} > 0 \forall \mathbf{z} \neq \mathbf{0}$;
- 2) $\|\mathbf{z}\|_{\Sigma} = 0$ iff $\mathbf{z} = \mathbf{0}$;
- 3) $\|a\mathbf{z}\|_{\Sigma} = |a| \cdot \|\mathbf{z}\|_{\Sigma}$ for a scalar a ;
- 4) $\|\mathbf{z}_1 + \mathbf{z}_2\|_{\Sigma} \leq \|\mathbf{z}_1\|_{\Sigma} + \|\mathbf{z}_2\|_{\Sigma}$.

where the vectors \mathbf{z}, \mathbf{z}_1 and \mathbf{z}_2 belong to the space \mathcal{Z} . The proof of these properties are provided as a supplement material with this manuscript.

Proposition 1: Mahalanobis norm $\|\mathbf{z}_i\|_{\Sigma}$ is a multivariate generalization of the Euclidean (or L_2) norm $\|\mathbf{z}_i\|_2$.

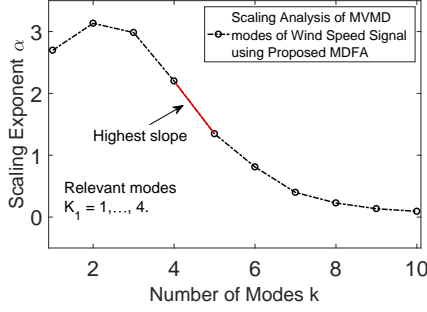


Fig. 2: Scaling exponent α_k of the MVMD modes (from wind signal), obtained via our MDFA, plotted against their index k .

Proof: To demonstrate that first we show that $\|\mathbf{z}_i\|_\Sigma$ reduces to $\|\mathbf{z}_i\|_2$ for uncorrelated multivariate data which involves two cases: Firstly, when $\Sigma = I_{m \times m}$ that denotes an identity matrix, $\|\mathbf{z}_i\|_\Sigma$ is given by

$$\|\mathbf{z}_i\|_{\Sigma=I_{m \times m}} = \sqrt{\mathbf{z}_i^T I_{m \times m}^{-1} \mathbf{z}_i} = \sqrt{\mathbf{z}_i^T \mathbf{z}_i} = \|\mathbf{z}_i\|_2. \quad (8)$$

Secondly, when $\Sigma = \sigma^T I_{m \times m}$ is a diagonal matrix where the vector $\sigma = [\sigma_1, \sigma_2, \dots, \sigma_m]^T$ contains channel variances, $\|\mathbf{z}_i\|_\Sigma$ is given by

$$\|\mathbf{z}_i\|_{\Sigma=\sigma^T I_{m \times m}} = \sqrt{\left(\frac{z_{i1}}{\sigma_1}\right)^2 + \dots + \left(\frac{z_{im}}{\sigma_m}\right)^2} = \|\bar{\mathbf{z}}_i\|_2 \quad (9)$$

where $\mathbf{z}_i = [z_{i1}, \dots, z_{im}]^T$ and $\bar{\mathbf{z}}_i = [\frac{z_{i1}}{\sigma_1}, \dots, \frac{z_{im}}{\sigma_m}]^T$.

Finally, in case of correlated multivariate data, Mahalanobis norm essentially computes the L_2 norm by un-correlating the variance normalized vector observations as depicted in Fig. 1. For a special case of bivariate data $\|\mathbf{z}_i\|_\Sigma$ can be rewritten as

$$\|\mathbf{z}_i\|_\Sigma = \frac{1}{\sqrt{1-\rho^2}} \sqrt{\|\bar{\mathbf{z}}_i\|_2^2 - \frac{2\rho z_{i1} z_{i2}}{\sigma_1 \sigma_2}} \quad (10)$$

where $\Sigma = \begin{pmatrix} \sigma_1^2 & \rho \sigma_1 \sigma_2 \\ \rho \sigma_1 \sigma_2 & \sigma_2^2 \end{pmatrix}$ and ρ is the correlation coefficient.

Based on *Proposition 1*, we utilize the generic (Mahalanobis) norm $\|\mathbf{y}_i - \tilde{\mathbf{y}}_i\|_\Sigma$ to formulate a purely multivariate fluctuation function $F_m^\Sigma(s)$ within MDFA, i.e.,

$$F_m^\Sigma(s) = \sqrt{\frac{1}{2sN_s} \sum_{v=1}^{2N_s} \sum_{i=vs+1}^{(v+1)s} (\mathbf{y}_i - \tilde{\mathbf{y}}_i)^T \Sigma^{-1} (\mathbf{y}_i - \tilde{\mathbf{y}}_i)}, \quad (11)$$

where covariance matrix Σ characterizes the interchannel dependencies within the detrend (or fluctuations) $\mathbf{y}_i - \tilde{\mathbf{y}}_i$.

Owing to the *Proposition 1*, it is clear that (5) is a special case of (11) for identity covariance matrix, i.e., uncorrelated input multichannel data. For more interesting cases involving multichannel data that exhibit cross-channel correlations, (11) provides more informative fluctuation scores.

In order to perform multichannel scaling analysis, $F_m^\Sigma(s)$ is computed for a varying time scales where generally the range $s = 4, \dots, 16$ is used [15]. Finally, a scaling exponent α is computed using power law representation of $F_m^\Sigma(s)$

$$F_m^\Sigma(s) = s^\alpha. \quad (12)$$

In practice, α is calculated based on the slope of the plot between $\ln F_m^\Sigma(s)$ and $\ln s$ because $\log_s F_m^\Sigma(s) = \frac{\ln F_m^\Sigma(s)}{\ln s}$ where \ln denotes the natural log operator.

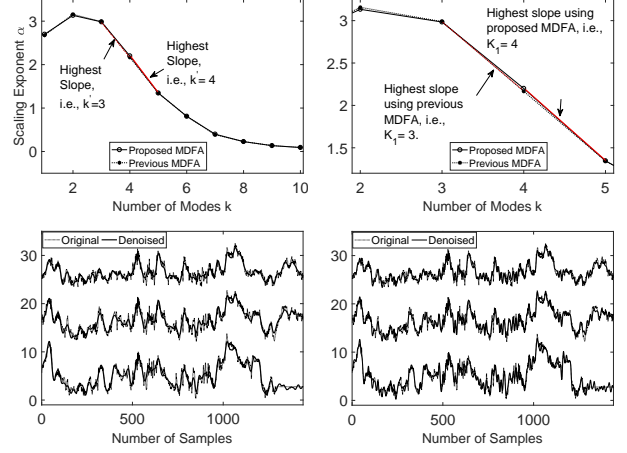


Fig. 3: Comparison of denoising performance of the proposed MDFA against the existing multichannel DFA [13].

B. Multivariate Signal Denoising Using MVMD and MDFA

Here, we present a multivariate signal denoising method that uses the proposed MDFA on the data-driven modes of noisy signal obtained from MVMD which involves following steps:

1) *Multiscale decomposition using MVMD*: Firstly, MVMD is used to decompose a noisy multivariate signal \mathbf{x}_i into an ensemble of K multichannel BLIMFs $\mathbf{u}_{k,i}$ which comprise of modulated multivariate oscillations of a common frequency component. Among those, initial BLIMFs contain low frequency (or smooth) oscillations whereas latter BLIMFs mostly comprise of high frequency fluctuations. This representation can be mathematically written as

$$\mathbf{x}_i = \sum_{k=1}^K \mathbf{u}_{k,i} = \sum_{k=1}^{K_1} \mathbf{u}_{k,i} + \sum_{k=K_1+1}^K \mathbf{u}_{k,i}, \quad \forall i = 1, \dots, N, \quad (13)$$

where $\{\mathbf{u}_{k,i}\}_{k=1}^{K_1}$ denotes the set of initial BLIMFs containing majority of (true) signal and $\{\mathbf{u}_{k,i}\}_{k=K_1+1}^K$ denotes the BLIMFs with predominant noise. Next, MDFA is used to detect the predominant noise modes, i.e., K_1 .

2) *Rejection of predominantly noisy BLIMFs using MDFA*: The proposed MDFA is used to identify and discard predominantly noisy BLIMFs based on (a) their higher frequency content and (b) absence of long-range auto-correlations. In this regard, the comparative analysis of the scaling exponents α_k , computed for each BLIMF $\mathbf{u}_{k,i}$ using (12), is performed. Understandably, α_k should decrease for every higher order BLIMF of the MVMD owing to the presence of increasingly high frequency fluctuations and decreasing long-range correlations that is evident from Fig. 2 that plots α_k for $K = 10$ MVMD modes of a noisy trivariate signal.

Let β_k denote the slope of the line connecting the exponents α_k and α_{k+1} of two consecutive modes, where

$$\beta_k = |\alpha_{k+1} - \alpha_k|. \quad (14)$$

The β_k quantifies the amount of change in the frequency of the fluctuations (or decrease in long-range correlations) when moving one mode to the other. That means, highest slope suggests maximum increase in frequency or maximum decrease in long-range correlations, i.e., largest increase in noise content. Consequently, the first mode after the highest slope, i.e., \mathbf{u}_{K_1+1} , marks the beginning of predominantly noisy modes where K_1 may be computed as follows

TABLE I: Input versus output SNR values of various comparative multivariate signal denoising methods on real signals.

Avg. Input SNR	-2	2	6	10	-2	2	6	10
Test Signal	Biv. Sofar Signal				Triv. Exercise Signal			
MWD bal.	6.86	11.11	14.56	18.66	7.24	8.75	10.03	11.26
unbal.	6.50	10.93	14.58	18.27	6.73	8.30	9.82	10.84
MWSD bal.	1.86	2.93	3.65	4.28	5.37	6.94	7.91	8.45
unbal.	1.51	2.52	3.42	4.05	4.63	6.57	7.74	8.31
MMD bal.	7.54	12.20	15.46	18.94	5.39	8.77	11.99	15.34
unbal.	8.05	11.72	15.03	18.91	5.12	8.67	11.99	15.18
MDD bal.	8.39	12.65	16.27	20.22	5.83	9.26	12.42	14.97
unbal.	8.56	12.02	16.50	19.38	5.39	9.32	11.95	14.73
Test Signal	Triv. Wind Signal				Quad. Synthetic Signal			
MWD bal.	9.13	11.25	12.07	12.99	6.69	10.33	13.62	17.05
unbal.	8.86	10.71	11.89	12.77	6.55	10.23	13.80	16.75
MWSD bal.	0.28	0.75	0.94	1.01	3.76	5.06	5.64	5.90
unbal.	0.18	0.70	0.89	0.99	3.06	4.35	5.42	5.73
MMD bal.	7.33	10.57	13.35	16.50	7.22	10.58	13.89	17.12
unbal.	7.54	10.61	13.56	16.26	7.78	10.47	13.75	16.92
MDD bal.	8.49	11.69	15.26	16.95	8.20	11.83	14.24	16.76
unbal.	8.33	11.64	14.61	16.84	8.31	11.42	14.09	15.80

$$K_1 = \underset{k}{\operatorname{argmax}} \{\beta_1, \dots, \beta_K\}. \quad (15)$$

Subsequently, the modes $\{\mathbf{u}_{k,i}\}_{k=K_1+1}^K$ are rejected as noise.

3) *Reconstruction*: The remaining multichannel BLIMFs $\{\mathbf{u}_{k,i}\}_{k=1}^{K_1}$, corresponding to relevant signal, may contain traces of noise which are removed by applying principal component analysis (PCA) separately on each multichannel mode, as suggested in [1]. In this regard, we employed heuristic approach [18] to identify the principal components. Finally, the denoised multivariate signal is obtained based on the post-processed selected relevant modes $\{\tilde{\mathbf{u}}_{k,i}\}_{k=1}^{K_1}$, as follows

$$\hat{\mathbf{s}}_i = \sum_{k=1}^{K_1} \tilde{\mathbf{u}}_{k,i} \quad \forall \quad i = 1, \dots, N, \quad (16)$$

where $\hat{\mathbf{s}}_i$ denotes the denoised multivariate signal.

V. RESULTS AND DISCUSSION

We evaluate the performance of the proposed multivariate denoising using DFA (MDD) method against the established state of the art methods which include multivariate wavelet denoising (MWD) [1], multivariate synchrosqueezing wavelet denoising (MWSD) [3] and multivariate denoising based on Mahalanobis distance (MMD) [7]. The input datasets used in our experiments include bivariate Sofar signal containing oceanographic float drift recordings [19], trivariate recordings of roll, pitch and yaw movements of the arm during weight lifting exercise, a trivariate wind speed signal obtained from a remote sight in Pakistan and a quadrivariate synthetic signal composed of Blocks, Bumps, Doppler and Heavy-Sine signals. These datasets were corrupted using multivariate additive wGn and were subsequently denoised using the comparative methods. The quality of the denoised signal is measured through the signal to noise ratio (SNR) and visual interpretation. The open source code of the MATLAB based implementation of the proposed MDD method is available online [20].

First, we compare the denoising performance of the proposed MDFA against the existing multichannel extension of DFA [13]. In this regard, scaling exponents (α_k) from both methods are plotted for $K = 10$ BLIMFs of noisy wind signal at input SNR 10 dB in Fig. 3 (top left). Observe from the zoomed-in view of the plot in Fig. 3 (top left) that maximum slope for [13] occurs between third and fourth mode (highlighted in dotted red line). Contrarily, using the proposed

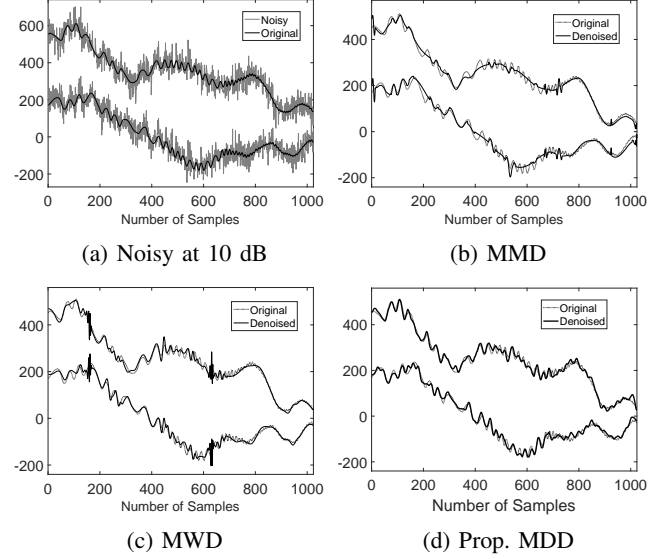


Fig. 4: Comparison of visual denoising results of the proposed MDD method against the state of the art methods for real Sofar signal at 10 dB input SNR.

MDFA, the maximum slope is exhibited between fourth and fifth mode (highlighted in solid red line). Observe from Fig. 3 (bottom right) that the denoised signal reconstructed from first four BLIMFs (as suggested by the proposed MDFA) is a closer estimate of the original signal (plotted in grey in the background) compared to that plotted in Fig. 3 (lower left) which is reconstructed from first three BLIMFs using [13].

Table I reports average output SNRs, of $J = 20$ realizations, from the comparative methods for all the input datasets (described above) at input SNR = -2, 2, 6 and 10 dB. At each input noise level, we consider balanced noise (i.e., same input SNRs for all channels) and unbalanced noise (i.e., different input SNRs in each channels) cases. To accentuate the best performing method, highest output SNRs are highlighted in bold for each input SNR. Observe that in most cases, the proposed MDD method yields highest output SNRs demonstrating the effectiveness of our method. Occasionally, at higher output SNRs, MMD outperforms our MDD method while MWD, generally regarded as the bench mark, remains competitive. Note that a comprehensive version of Table I (i.e., Table II) is given in the supplement material provided with this article.

Finally, we inspect the visual quality of the reconstructed signal by displaying the denoised Sofar signals in Fig. 4 along with the noisy version at input SNR = 10 dB. Observe that proposed method yields best estimate of the original signal (plotted in dotted line in the background) whereas MMD and MWD miss important signal details and yield artifacts.

VI. CONCLUSION

We have proposed a novel multivariate signal denoising method that is based on data driven multiscale representation and statistical signal properties. A novel and generic multichannel extension of detrended fluctuation analysis (DFA) underpins our denoising method which has been demonstrated to outperform existing approaches owing to the full utilization of interchannel correlations within input data via Mahalanobis distance measure.

REFERENCES

- [1] M. Aminghafari, N. Cheze, and J.-M. Poggi, "Multivariate denoising using wavelets and principal component analysis," *Computational Statistics & Data Analysis*, vol. 50, no. 9, pp. 2381–2398, 2006.
- [2] D. L. Donoho, I. M. Johnstone, G. Kerkycharian, and D. Picard, "Wavelet shrinkage: asymptopia?," *Journal of the Royal Statistical Society. Series B (Methodological)*, pp. 301–369, 1995.
- [3] A. Ahrabian and D. P. Mandic, "A class of multivariate denoising algorithms based on synchrosqueezing," *IEEE Trans. Signal Processing*, vol. 63, no. 9, pp. 2196–2208, 2015.
- [4] N. Rehman and D. P. Mandic, "Multivariate empirical mode decomposition," *Proceedings of the Royal Society A: Mathematical, Physical and Engineering Sciences*, vol. 466, no. 2117, pp. 1291–1302, 2009.
- [5] N. Rehman, K. Naveed, M. Safdar, S. Ehsan, and K. McDonald-Maier, "Dynamically sampled multivariate empirical mode decomposition," *Electronics Letters*, vol. 51, no. 24, pp. 2049–2051, 2015.
- [6] H. Hao, H. Wang, and N. Rehman, "A joint framework for multivariate signal denoising using multivariate empirical mode decomposition," *Signal Processing*, vol. 135, pp. 263–273, 2017.
- [7] N. ur Rehman, B. Khan, and K. Naveed, "Data-driven multivariate signal denoising using mahalanobis distance," *IEEE Signal Processing Letters*, vol. 26, no. 9, pp. 1408–1412, 2019.
- [8] K. Dragomiretskiy and D. Zosso, "Variational mode decomposition," *IEEE transactions on signal processing*, vol. 62, no. 3, pp. 531–544, 2014.
- [9] N. ur Rehman and H. Aftab, "Multivariate variational mode decomposition," *IEEE Transactions on Signal Processing*, vol. 67, no. 23, pp. 6039–6052, 2019.
- [10] P. Cao, H. Wang, and K. Zhou, "Multichannel signal denoising using multivariate variational mode decomposition with subspace projection," *IEEE Access*, vol. 8, pp. 74039–74047, 2020.
- [11] C.-K. Peng, S. V. Buldyrev, S. Havlin, M. Simons, H. E. Stanley, and A. L. Goldberger, "Mosaic organization of dna nucleotides," *Physical review e*, vol. 49, no. 2, p. 1685, 1994.
- [12] Y. Liu, G. Yang, M. Li, and H. Yin, "Variational mode decomposition denoising combined the detrended fluctuation analysis," *Signal Processing*, vol. 125, pp. 349–364, 2016.
- [13] H. Xiong and P. Shang, "Detrended fluctuation analysis of multivariate time series," *Communications in Nonlinear Science and Numerical Simulation*, vol. 42, pp. 12–21, 2017.
- [14] C.-K. Peng, S. V. Buldyrev, S. Havlin, M. Simons, H. E. Stanley, and A. L. Goldberger, "Mosaic organization of dna nucleotides," *Physical review e*, vol. 49, no. 2, p. 1685, 1994.
- [15] J. W. Kantelhardt, E. Koscielny-Bunde, H. H. Rego, S. Havlin, and A. Bunde, "Detecting long-range correlations with detrended fluctuation analysis," *Physica A: Statistical Mechanics and its Applications*, vol. 295, no. 3–4, pp. 441–454, 2001.
- [16] A. Mert and A. Akan, "Detrended fluctuation thresholding for empirical mode decomposition based denoising," *Digital Signal Processing*, vol. 32, pp. 48–56, 2014.
- [17] S. Leistedt, M. Dumont, J.-P. Lanquart, F. Jurysta, and P. Linkowski, "Characterization of the sleep eeg in acutely depressed men using detrended fluctuation analysis," *Clinical neurophysiology*, vol. 118, no. 4, pp. 940–950, 2007.
- [18] D. Karlis, G. Saporta, and A. Spinakis, "A simple rule for the selection of principal components," *Communications in Statistics-Theory and Methods*, vol. 32, no. 3, pp. 643–666, 2003.
- [19] P. Richardson, J. Price, D. Walsh, L. Armi, and M. Schröder, "Tracking three meddies with sofar floats," *Journal of Physical Oceanography*, vol. 19, no. 3, pp. 371–383, 1989.
- [20] K. Naveed, "Multivariate signal denoising using generic multichannel dfa," 2020, [Online], *Matlab Central File Exchange*, vol. <https://www.mathworks.com/matlabcentral/fileexchange/78062-multivariate-signal-denoising-using-generic-multichannel-dfa>.

VII. SUPPLEMENT MATERIAL

A. Mahalanobis Distance as a Norm

Let Σ be a symmetric covariance matrix (of size $m \times m$) corresponding to multivariate observations $\mathbf{z}_i \in \mathcal{R}^m \forall i = 1, \dots, N$. The Mahalanobis distance is defined as follows

$$\|\mathbf{z}_i\|_{\Sigma} = \sqrt{\mathbf{z}_i^T \Sigma^{-1} \mathbf{z}_i}, \quad (17)$$

The properties of $\|\cdot\|_{\Sigma}$ required to define it as a norm, stated in *Definition 1*, are proved below:

We know that inverse of a symmetric and positive definite matrix, $\Sigma = \Sigma^T \succ 0$, is also symmetric and positive definite matrix $\Sigma^{-1} = \Sigma^{-1T} \succ 0$; hence, the only way

$$\|\mathbf{z}_i\|_{\Sigma} = 0, \quad \text{iff} \quad \mathbf{z}_i = \mathbf{0}. \quad (18)$$

Also, since $\|\mathbf{z}_i\|_{\Sigma} = \sqrt{\mathbf{z}_i^T \Sigma^{-1} \mathbf{z}_i}$ is quadratic function with a positive definite matrix $\Sigma^{-1} \succ 0$,

$$\|\mathbf{z}_i\|_{\Sigma} > 0, \quad \forall \quad \mathbf{z}_i \neq \mathbf{0}. \quad (19)$$

It is also trivial to show that $\|a\mathbf{z}_i\|_{\Sigma} = |a| \cdot \|\mathbf{z}_i\|_{\Sigma}$ for a scalar a , as follows

$$\|a\mathbf{z}_i\|_{\Sigma} = \sqrt{(a\mathbf{z}_i)^T \Sigma^{-1} (a\mathbf{z}_i)} = a \sqrt{\mathbf{z}_i^T \Sigma^{-1} \mathbf{z}_i} = |a| \cdot \|\mathbf{z}_i\|_{\Sigma} \quad (20)$$

To prove the triangular inequality, we perform spectral decomposition of symmetric matrices that results in a diagonal $m \times m$ matrix $\Lambda = \text{diag}(\lambda_1, \lambda_2, \dots, \lambda_n)$ and an orthogonal $m \times m$ matrix Q (i.e., $Q^T Q = I_{m \times m}$ where $I_{m \times m}$ denotes an identity matrix), such that $Q^T = Q^{-1}$ and

$$\Sigma = Q^T \Lambda Q. \quad (21)$$

By definition, Σ is positive-definite matrix that means $\lambda_1 > 0, \lambda_2 > 0, \dots, \lambda_m > 0$, hence a matrix S may be defined

$$S = \Lambda^{\frac{1}{2}} Q = \text{diag}(\sqrt{\lambda_1}, \sqrt{\lambda_2}, \dots, \sqrt{\lambda_n}) Q, \quad (22)$$

such that

$$\Sigma = S^T S. \quad (23)$$

By using (22) in (17), we get

$$\|\mathbf{z}_i\|_{\Sigma} = \sqrt{(S\mathbf{z}_i)^T (S\mathbf{z}_i)}, \quad (24)$$

Now, let us set $\tilde{\mathbf{z}}_i = S\mathbf{z}_i$ then

$$\|\mathbf{z}_i\|_{\Sigma} = \sqrt{\tilde{\mathbf{z}}_i^T \tilde{\mathbf{z}}_i} = \|\tilde{\mathbf{z}}_i\|_2, \quad (25)$$

Following from (25), it is straight forward to show that

$$\begin{aligned} \|\mathbf{z}_1 + \mathbf{z}_2\|_{\Sigma} &= \sqrt{(\mathbf{z}_1 + \mathbf{z}_2)^T \Sigma^{-1} (\mathbf{z}_1 + \mathbf{z}_2)} \\ &= \sqrt{(\mathbf{z}_1 + \mathbf{z}_2)^T S^T S (\mathbf{z}_1 + \mathbf{z}_2)} \\ &= \sqrt{(S\mathbf{z}_1 + S\mathbf{z}_2)^T (S\mathbf{z}_1 + S\mathbf{z}_2)} \\ &= \sqrt{(\tilde{\mathbf{z}}_1 + \tilde{\mathbf{z}}_2)^T (\tilde{\mathbf{z}}_1 + \tilde{\mathbf{z}}_2)} \\ &= \|\tilde{\mathbf{z}}_1 + \tilde{\mathbf{z}}_2\|_2, \end{aligned} \quad (26)$$

Since, we already know that L_2 follows the traingular inequality which means

$$\|\tilde{\mathbf{z}}_1 + \tilde{\mathbf{z}}_2\|_2 \leq \|\tilde{\mathbf{z}}_1\|_2 + \|\tilde{\mathbf{z}}_2\|_2 \quad (27)$$

and from (25)-(28), we is can be shown that

$$\|\mathbf{z}_1 + \mathbf{z}_2\|_{\Sigma} \leq \|\mathbf{z}_1\|_{\Sigma} + \|\mathbf{z}_2\|_{\Sigma} \quad (28)$$

TABLE II: Input versus output SNR values of various comparative multivariate signal denoising methods on real signals. This table is an extensive version of *Table I* where we also show output SNRs of each channel (in both balanced and unbalanced noise case) along with the average reconstructed SNRs of the multivariate signal which are also reported within the manuscript.

Avg. Input SNR	-2			2				6				10						
Test Signal	Sofar Bivariate Signal																	
Channels	C1	C2	Avg		C1	C2	Avg		C1	C2	Avg		C1	C2	Avg			
Inp. SNR (Balanced)	-2	-2	-2		2	2	2		6	6	6		10	10	10			
Inp. SNR (Unbalanced)	-3	-1	-2		1	3	2		5	7	6		9	11	10			
MWD	7.02	6.71	6.86		11.05	11.17	11.11		14.69	14.45	14.56		18.76	18.57	18.66			
	5.70	7.50	6.50		10.13	11.87	10.93		13.69	15.65	14.58		17.43	19.28	18.27			
MWSD	1.52	2.22	1.86		2.69	3.18	2.93		3.57	3.72	3.65		4.41	4.17	4.28			
	1.11	1.94	1.51		2.25	2.81	2.5273		3.34	3.50	3.42		4.06	4.04	4.05			
MMD	7.42	7.68	7.54		12.12	12.31	12.20		15.33	15.61	15.46		18.86	19.03	18.94			
	7.27	9.00	8.05		10.92	12.69	11.72		14.19	16.06	15.03		18.02	20.01	18.91			
MDD	8.35	8.45	8.39		12.70	12.62	12.65		16.47	16.10	16.27		20.17	20.29	20.22			
	7.72	9.59	8.56		11.17	13.05	12.02		15.68	17.48	16.50		18.50	20.46	19.38			
Test Signal	Trivariate Health Monitoring Signal																	
Channels	C1	C2	C3	Avg		C1	C2	C3	Avg		C1	C2	C3	Avg				
Inp. SNR (Balanced)	-2	-2	-2	-2		2	2	2	2		6	6	6	6				
Inp. SNR (Unbalanced)	-3	-2	-1	-2		1	2	3	2		5	6	7	6				
MWD	8.29	2.16	7.33	7.24		10.14	2.13	9.50	8.75		12.48	0.48	12.13	10.03				
	7.50	3.01	6.68	6.73		9.45	2.73	8.78	8.30		11.81	1.52	11.38	9.82				
MWSD	5.00	4.89	6.02	5.37		6.44	6.08	7.91	6.94		7.18	6.93	9.40	7.91				
	4.35	4.27	5.11	4.63		6.07	5.86	7.53	6.57		7.03	6.83	9.18	7.74				
MMD	5.62	5.06	5.11	5.39		8.89	8.82	8.60	8.77		12.12	12.16	11.80	11.99				
	4.57	5.43	6.00	5.12		8.11	8.77	9.61	8.67		11.43	12.41	12.86	11.99				
MDD	5.76	5.80	5.94	5.83		9.20	9.01	9.42	9.26		12.37	12.81	12.51	12.42				
	4.68	5.15	6.71	5.39		8.67	9.80	10.38	9.32		11.47	11.81	12.88	11.95				
Test Signal	Trivariate Wind Speed Signal																	
Channels	C1	C2	C3	Avg		C1	C2	C3	Avg		C1	C2	C3	Avg				
Inp. SNR (Balanced)	-2	-2	-2	-2		2	2	2	2		6	6	6	6				
Inp. SNR (Unbalanced)	-3	-2	-1	-2		1	2	3	2		5	6	7	6				
MWD	9.23	9.43	8.57	9.13		11.33	11.93	10.31	11.25		12.28	12.85	10.76	12.07				
	8.93	9.13	8.39	8.86		10.67	11.37	9.96	10.71		12.08	12.61	10.68	11.89				
MWSD	0.21	0.32	0.40	0.28		0.67	0.81	0.82	0.75		0.88	0.96	1.02	0.94				
	0.12	0.21	0.29	0.18		0.64	0.71	0.80	0.70		0.85	0.90	0.97	0.89				
MMD	7.39	7.24	7.37	7.33		10.68	10.48	10.50	10.57		13.41	13.42	13.14	13.35				
	7.00	7.75	8.49	7.54		10.17	10.69	11.55	10.61		13.32	13.63	14.01	13.56				
MDD	8.42	8.46	8.70	8.49		11.80	11.58	11.67	11.69		15.54	15.14	14.96	15.26				
	7.70	8.55	9.56	8.33		11.22	11.79	12.42	11.64		14.38	14.70	14.97	14.61				
Test Signal	Synthetic Quadrivariate Signal																	
Channels	C1	C2	C3	C4	Avg		C1	C2	C3	C4	Avg		C1	C2	C3	C4	Avg	
Inp. SNR (Balanced)	-2	-2	-2	-2	-2		2	2	2	2	2		6	6	6	6	6	
Inp. SNR (Unbalanced)	-3	-2	-1	0	-2		0	1	2	3	2		4	5	8	9	6	
MWD	6.73	6.68	7.04	6.35	6.69		10.08	10.50	10.78	10.09	10.33		13.27	13.68	14.27	13.34	13.62	
	4.78	5.42	7.93	8.34	6.55		8.40	9.50	11.72	11.73	10.23		11.95	13.11	15.59	14.99	13.80	
MWSD	1.37	3.18	5.44	6.44	3.76		2.08	4.35	7.64	8.86	5.06		2.37	4.83	8.80	10.30	5.64	
	0.89	2.64	4.58	5.15	3.06		1.67	3.74	6.37	7.57	4.35		2.25	4.68	8.46	9.61	5.42	
MMD	6.77	6.40	7.57	7.73	7.22		9.93	10.23	10.95	11.11	10.58		13.01	13.88	14.49	14.31	13.89	
	5.89	6.18	9.42	9.90	7.78		8.45	9.44	11.96	12.63	10.47		11.57	12.69	15.26	16.38	13.75	
MDD	7.72	7.90	8.89	8.24	8.20		11.47	11.39	13.08	11.33	11.83		13.27	14.12	16.43	13.64	14.24	
	6.31	7.06	10.45	9.94	8.31		9.56	10.42	13.73	12.44	11.42		12.18	12.72	17.97	14.47	14.09	